J Seismol (2013) 17:753–769
DOI 10.1007/s10950-012-9352-1

ORIGINAL ARTICLE

Seismic discrimination of the 2009 North Korean nuclear explosion based on regional source spectra

Tae-Kyung Hong

Received: 1 July 2012 / Accepted: 27 November 2012 / Published online: 29 December 2012

Abstract Seismic discrimination of an underground nuclear explosion (UNE) based on regional waveforms in continental margins is challenging due to large variations among waveforms. The 2009 North Korean UNE test was conducted in the far eastern Eurasian plate. The UNE was recorded by densely-located regional seismic stations, and regional waveforms exhibit highly path-dependent amplitude and arrival time features due to complex crustal structures. Regional source spectra are calculated by correcting for the path effects on the waveforms. A two-step approach is proposed for stable inversion of source-spectral parameters and path parameters. Characteristic overshoot features are observed in the source spectra, particularly strong in *Pn*. The path parameter, *Q*, is determined uniquely regardless of the source-spectral model implemented, which suggests stable separation of path effects from waveform records. The estimated source spectra fit well to a theoretical UNE source-spectral model. The fitness between the estimated and theoretical source-spectral models allows us to discriminate UNEs from natural earthquakes. Also, the *P/S* source-spectral ratio is observed to be an effective discriminant of UNE.

Keywords Seismic discrimination · Underground nuclear explosion · North Korea · Continental margin

1 Introduction

Seismic analyses play an important role in the monitoring of underground nuclear explosions (UNEs). Various seismic methods have been proposed for discriminating UNEs from natural earthquakes, which include comparison between body-wave magnitudes and surface-wave magnitudes (e.g., Taylor et al. 1989; Bonner et al. 2008), comparison of *P/S* amplitude ratio (e.g., Xie and Patton 1999; Richards and Kim 2007), analysis of energy contents in surface waves (Brune and Pomerory 1963), analysis of spectral energy (Weichert 1971), and analysis of moment-tensor components (Ford et al. 2009).

Small and moderate-sized UNEs are observed only up to regional distances in which seismic waves are highly influenced by crustal structures (e.g., Walter et al. 2007; Hong et al. 2008; Koper et al. 2008; Zhao et al. 2008; Patton and Taylor 2008;

T.-K. Hong (✉)
Department of Earth System Sciences,
Yonsei University, 50 Yonsei-ro, Seodaemun-gu,
Seoul 120-749, South Korea
e-mail: tkhong@yonsei.ac.kr

Chun and Henderson 2009; Hong 2010b). Stable discrimination of UNEs at regional distances is a long-standing issue, especially for regions with complex crustal structures such as continental margins. It is known that regional waves are highly variable in the continental margins depending on the path (e.g., Kennett and Furumura 2001; Hong et al. 2008; Hong 2012; Hong and Lee 2012). Also, seismologists often observe strong S wave trains from UNEs in regional distances (e.g., Xie and Patton 1999; Patton 2001; Hong and Xie 2005; Kim and Richards 2007; Bonner et al. 2008; Zhao et al. 2008; Hong 2010b). These features hinder stable discrimination of UNEs based on seismic waveforms at regional distances in and around the continental margins.

The highly path-dependent seismic waveforms cause difficulty in application of conventional methods for discrimination of UNEs. Thus, it is desirable to use path-corrected source spectra of the UNEs for stable discrimination. There have been attempts to determine regional-wave source spectra by correcting the waveform spectra for seismic attenuation along paths (e.g., Mueller and Murphy 1971; Burdick et al. 1984; Fisk 2007). Here, various source-spectral models have been considered (e.g., Mueller and Murphy 1971; Aki et al. 1974; Lay et al. 1984; Sereno et al. 1988; Denny and Johnson 1991). However, such seismic discrimination of UNEs based on the path-corrected source spectra has been rarely conducted in the continental margins, and its validity remains unclear.

North Korea conducted two moderate-sized UNE tests in 2006 and 2009. The UNEs were detonated at the far eastern margin of the Eurasian plate (Richards and Kim 2007; Hong et al. 2008; Ford et al. 2009; Shin et al. 2010). The events were well recorded by densely-located regional seismic networks in Korea, Japan, and China. The UNEs provide us with a unique opportunity to examine the feasibility of the discrimination method using complex high-frequency regional waveforms.

In this study, we investigate the characteristics of regional waveforms from the UNEs. We determine the regional source spectrum of the 2009 UNE from the regional waveforms. The inverted parameters are compared among different source models, and their validity is examined. The path parameters for common stations are compared between the UNEs to verify the inversion method. Also, seismic discrimination based on the source spectra is performed for the 2009 UNE.

2 Data and geology

The North Korean UNE tests were conducted on October 9, 2006 and May 25, 2009 at nearby locations that are separated by about 8.9 km (Table 1). The magnitudes (m_b) of the UNEs are 4.2 and 4.7. These UNEs were well observed by regional seismic networks (Fig. 1). The scalar isotropic moments are reported to be $\sim 3 \times 10^{14}$ Nm for the 2006 UNE (Walter et al. 2007; Hong and Rhie 2009) and 1.8×10^{15} Nm for the 2009 UNE (Ford et al. 2009).

The Korean Peninsula is located in the far eastern margin of the Eurasia plate and is composed of three precambrian massif blocks and two intervening fold belts (e.g., Chough et al. 2000). The Korean Peninsula is underlain by a typical continental crust with a mid-crustal seismic discontinuity (He and Hong 2010). Toward the east, the continental crust in the Korean Peninsula changes to transitional or oceanic crusts in the East Sea (Sea of Japan) (e.g., Hong et al. 2008; Hong 2010a). It is reported that structural variations in the crust cause high modulation in regional phases (e.g., Kennett and Furumura 2001; Hong et al. 2008; Hong 2011).

We collect 801 regional seismograms for the 2009 UNE from seismic stations in South Korea, Japan, and China (Fig 1). The epicentral distances are 342–1884 km. The seismic stations are equipped with either broad-band or short-period velocity seismometers and accelerometers. The sampling rates of records from the Korean stations are 0.01 s, and those from the Chinese and

Table 1 Event information of the 2006 and 2009 North Korean UNEs and a nearby earthquake in 2002

Event	Date	Time	Lat (°N)	Lon (°E)	m_b
UNE 2009	05/25/2009	00:54:43	41.30	129.03	4.7
UNE 2006	10/09/2006	01:35:27	41.29	129.13	4.2
EQ 2002	16/04/2002	22:52:38	40.66	128.65	4.1

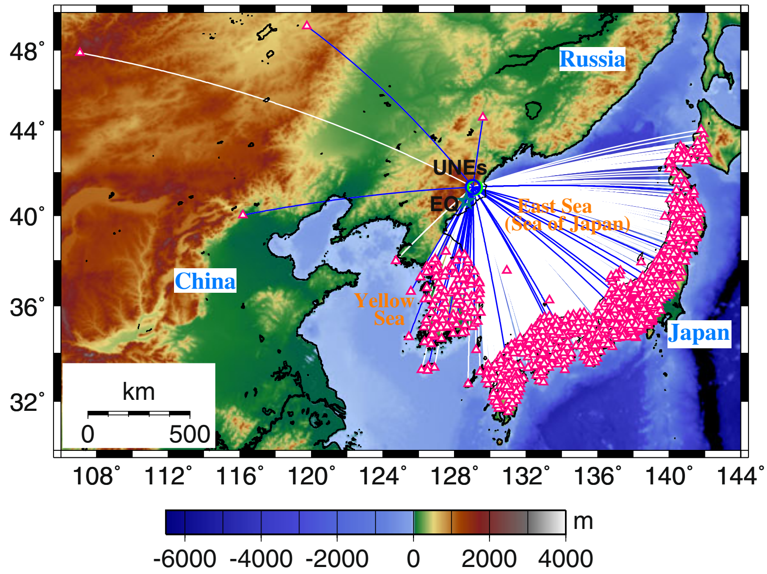

Fig. 1 The locations of events and stations on a topographic map. The epicenter of the 2006 North Korean UNE is marked with a *green circle*, that of the 2009 UNE with a *blue circle*, and that of the 2002 earthquake (*EQ*) with an *open star*. The stations are marked with *red triangles*. The great-circle paths from the 2009 UNE to stations are presented with *solid lines*. A total of 801 seismic waveforms are collected for an analysis of the 2009 UNE. The two UNEs are separated by ∼82 km. The focal depth of the earthquake is 10 km

Japanese stations are 0.05 s. The raw waveforms are corrected for instrument responses and then converted to ground displacements (Fig. 2).

3 Regional waveforms

Some selected regional waveform records are presented in Fig. 2. We find significant path-dependent variations in the amplitudes and apparent velocities of the phases. In particular, we find strong attenuation of crustal-guided shear waves (*Lg*) for paths across the East Sea in which transitional or oceanic crusts are present (Hong 2010a). A similar feature is observed in the crustal *P* waves (*Pg*). We observe relatively prominent mantle-lid *P* waves (*Pn*) at most stations. On the other hand, the mantle-lid *S* waves (*Sn*) are weak at distances greater than about 1,000 km.

The strong attenuations of *Pg* and *Lg* along the paths across the East Sea suggests the presence of a laterally inhomogeneous crustal structure. The prominent *Pn* phase suggests strong excitation of *P* energy from the source. The signal-to-noise ratios of *Pn* phase are as high as 2–5 in most records (Fig. 3). The strong *Pn* phase appears to be useful for inference of the source properties.

The vertical displacement waveforms for the 2006 and 2009 UNEs at eight common stations are compared to examine the similarity of waveforms (Fig. 4). The stations are selected to cover various raypaths and azimuths in the Korean Peninsula. Paths to stations in the east coast of the Korean Peninsula (CHC, DAG) cross major oceanic crustal segments, while those to the west coast (BRD, SES) largely (or, entirely) cross continental crust. Also, three pairs of stations with similar azimuths (SEO-SES, CHC-KWJ, and DGY-DAG) are prepared to examine distance-dependent features. Stations at farther distances have longer continental paths than those at nearer distances. A bandpass filter between 0.8 and 2 Hz is applied to the waveform records.

The phase compositions in wave trains appear to vary significantly with azimuth and path. We find strong development of *Lg* phase along the continental paths, while weak or rare *Lg* is observed along the suboceanic paths. We also observe that the phase composition is different

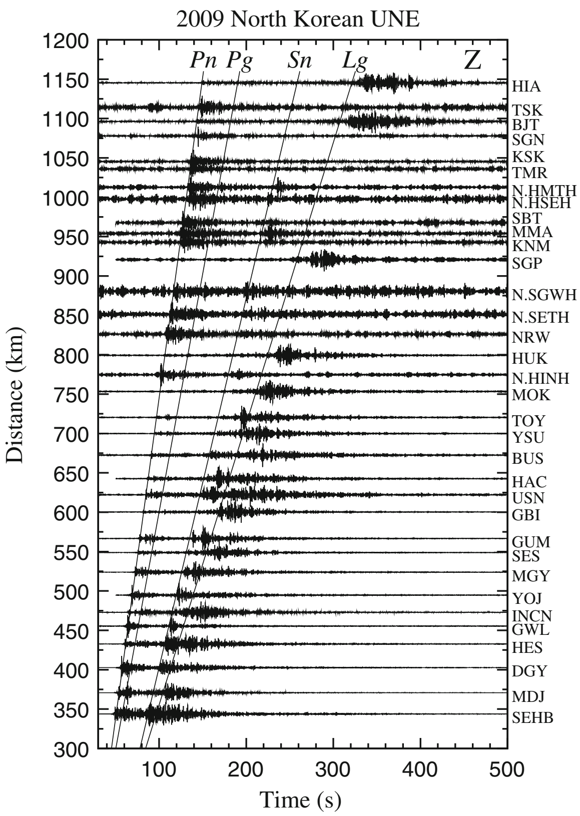

Fig. 2 Vertical displacement record sections for the 2009 North Korean UNE from some selected paths that are marked with *blue lines* in Fig. 1. Each record section is normalized by its maximum amplitude. The arrival times of major regional phases (*Pn, Pg, Sn, Lg*) are marked with *solid lines*. The regional phases are observed to be influenced by discriminative path-dependent attenuation

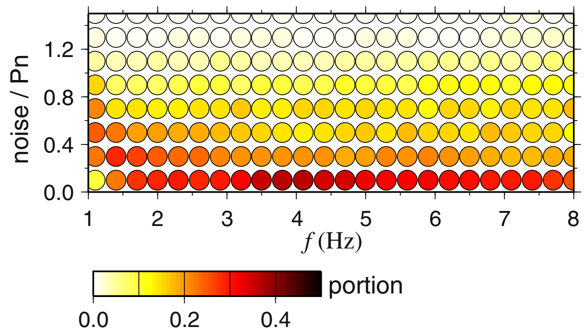

Fig. 3 Distribution of the inverse of *Pn* signal-to-noise ratios of collected waveforms that are strong enough at frequencies between 1 and 8 Hz for a source-spectral analysis. The ambient noise field is collected from 20-s-long record sections before *Pn* arrivals

between the stations with similar azimuths (SEO-SES, CHC-KWJ, and DGY-DAG). We find strong *Lg* waves in stations with longer continental paths. For instance, stations CHC and DGY display weak *Lg* and strong *Sn*, while stations KWJ and DAG present strong *Lg* and weak *Sn*.

The arrival times of major phases are observed to be similar between the UNEs, supporting hypocentral proximity between the UNEs. We, however, find large differences in wave train compositions and relative phase amplitudes between the UNEs. As a result, the *P/S* amplitude ratios at common stations appear to be highly different between the UNEs. For instance, at station DGY, the peak *S* amplitude is larger than the peak *P* amplitude in the record for the 2006 UNE, while the peak *P* amplitude is larger than the peak *S* amplitude in the record for the 2009 UNE (Fig. 4e). Similar observations are found in other UNEs (Hong 2010b).

The waveform variations between the UNEs may be associated with changes in raypaths or differences in source-region geology (Rodgers et al. 2010). This observation suggests that direct comparison of peak amplitudes of waveforms may not be suitable to constrain the relative strength between the UNEs. Also, it is suggested that stable seismic discrimination may be difficult to achieve with records from sparsely-located networks.

4 Theory

The high variability of waveforms by path makes it difficult to use the simple *P/S* amplitude ratios of single seismic records for discrimination of UNE. It is desirable to use the energy directly excited from the source for stable discrimination. In this study, we discriminate the UNE sources based on the source spectra.

The displacement spectrum of seismic waves at station i, $A_i(f)$, can be expressed as (Sereno et al. 1988; Xie and Patton 1999)

$$A_i(f) = S(f)G(d_i)\exp\left(-\frac{\pi f d_i}{v_g Q_i(f)}\right)e_i(f), \qquad (1)$$

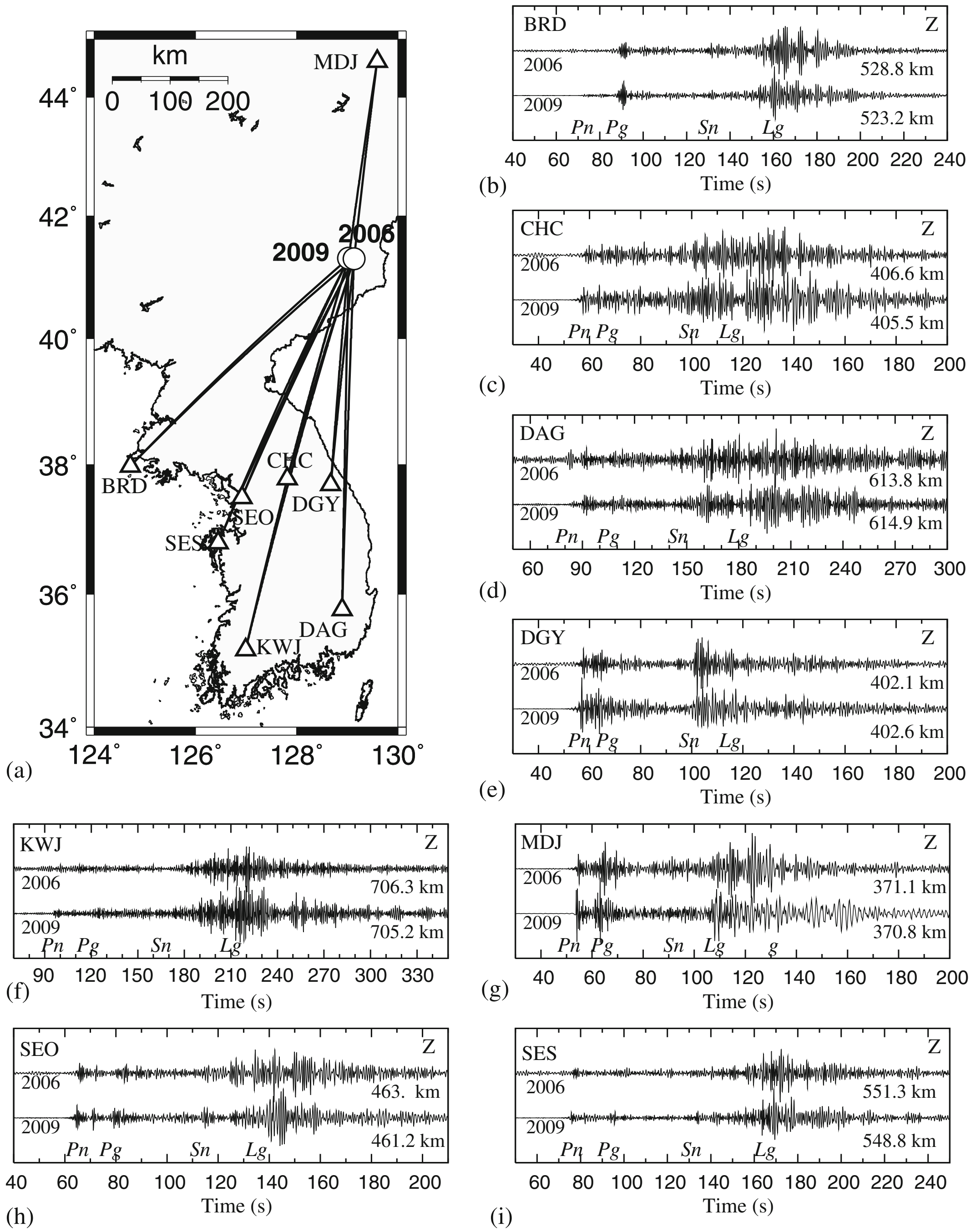

Fig. 4 Comparisons of waveforms at common stations between the 2006 and 2009 North Korean UNEs: (**a**) map for events and stations, and the vertical displacement waveforms for stations (**b**) BRD, (**c**) CHC, (**d**) DAG, (**e**) DGY, (**f**) KWJ, (**g**) MDJ, (**h**) SEO, and (**i**) SES. The epicenters of the 2006 and 2009 North Korean UNEs are marked with *circles*, and the locations of stations are with indicated by *triangles*. The great-circle paths are presented by *solid lines*. The epicentral distance and major regional phases are denoted in each record section. The record sections are bandpass-filtered between 0.8 and 2 Hz. The waveforms are observed to be different between the pairs of stations

where f is the frequency, $S(f)$ is the source spectrum, d_i is the epicentral distance, $G(d_i)$ is the geometrical spreading term, $Q_i(f)$ is the quality factor along the path to station i, v_g is the group velocity, and $e_i(f)$ is the cumulative effect of unaccounted factors along the path. The influence of the unaccounted factors is trivial compared to that of the major source and path factors. The quality factor $Q_i(f)$ can be written as

$$Q_i(f) = Q_{0,i} f^{\eta_i}, \tag{2}$$

where $Q_{0,i}$ is the quality factor at 1 Hz, and η_i is the power-law frequency dependence.

The geometrical spreading term, $G(d_i)$, is given by

$$G(d_i) = (d_0/d_i)^{\gamma}\, d_0^{-1}, \tag{3}$$

where γ is the decay rate of phase, and d_0 is the reference distance. We set $d_0 = 100$ km and $\gamma = 0.5$ for Lg, and $d_0 = 1$ km and $\gamma = 1.1$ for Pn, Pg and Sn (Zhu et al. 1991; Walter and Taylor 2002; Hong and Rhie 2009). The source spectrum, $S(f)$, is given by (Mueller and Murphy 1971; Xie and Patton 1999)

$$S(f) = \frac{M_0}{4\pi\rho_s v_s^3\sqrt{1+(1-2\xi)f^2/f_c^2+\xi^2 f^4/f_c^4}}, \tag{4}$$

where M_0 is the moment, ξ is the overshoot parameter, f_c is the corner frequency, ρ_s is the density in the source region, and v_s is the phase velocity in the source region.

Equation 1 can be recast to be a linear system as

$$\mathbf{a} = \mathbf{Bm}, \tag{5}$$

where $\mathbf{a}$ is a column vector for observed spectral amplitudes, $\mathbf{B}$ is a matrix for linear operators, and $\mathbf{m}$ is the model vector. The column vector $\mathbf{a}$ is given by

$$\mathbf{a} = \left[\ln A_1(f_1), \ln A_1(f_2), \cdots, \ln A_1(f_m), \ln A_2(f_1), \ln A_2(f_2), \cdots, \ln A_n(f_m)\right]^T, \tag{6}$$

where m is the number of discrete frequencies, and n is the number of stations. The total number of rows in vector $\mathbf{a}$ is $m \times n$. The model vector $\mathbf{m}$ is given by

$$\mathbf{m} = \left[M_0, f_c, \xi, Q_{0,1}, \eta_1, Q_{0,2}, \eta_2, \cdots, Q_{0,n}, \eta_n\right]^T, \tag{7}$$

where M_0, f_c, ξ, $Q_{0,i}$ and η_i are unknown parameters to be determined. Parameters M_0, f_c, and ξ represent source properties, and parameters $Q_{0,i}$, and η_i present path properties. Here, M_0 is an apparent moment that varies with the size of time window and frequency band applied. On the other hand, parameters f_c, ξ and Q are determined uniquely for each phase.

For each regional phase, discrete sets of M_0, f_c, and ξ are prepared. The path parameters $Q_{0,i}$ and η_i are determined using the LSQR inversion method (the sparse linear equations and sparse least squares method; Paige and Saunders 1982) for given discrete sets of M_0, f_c, and ξ. A set of source parameters (M_0, f_c, and ξ) yielding the minimum misfit error between the observed and theoretical source spectra is determined. The path parameters ($Q_{0,i}$, η_i) associated with the best-fit source parameters are determined subsequently. It is noteworthy that parameters M_0 and Q are determined nonuniquely in the inversion due to their mutual trade-offs; a high M_0 incorporates a set of low Q in the inversion, and vice versa.

To avoid the nonunique determination of model parameters, we introduce a two-step inversion approach (Hong and Rhie 2009). In the first step of inversion, we determine M_0 that yields the Q values consistent with previous studies (Kim et al. 1999; Chung and Sato 2001; Hong and Rhie 2009; Hong 2010a). Here, we apply a grid-searching scheme to determine an optimum M_0 that yields the minimum residual between inverted and reported Q values. In the second step, we invert f_c and ξ with implementation of the predetermined apparent moment (M_0). A set of f_c and ξ yielding the minimum misfit error between the inverted and theoretical source spectra is searched. The path parameter Q is newly determined at every inversion of f_c and ξ. The Q parameters inverted with the best-fit source

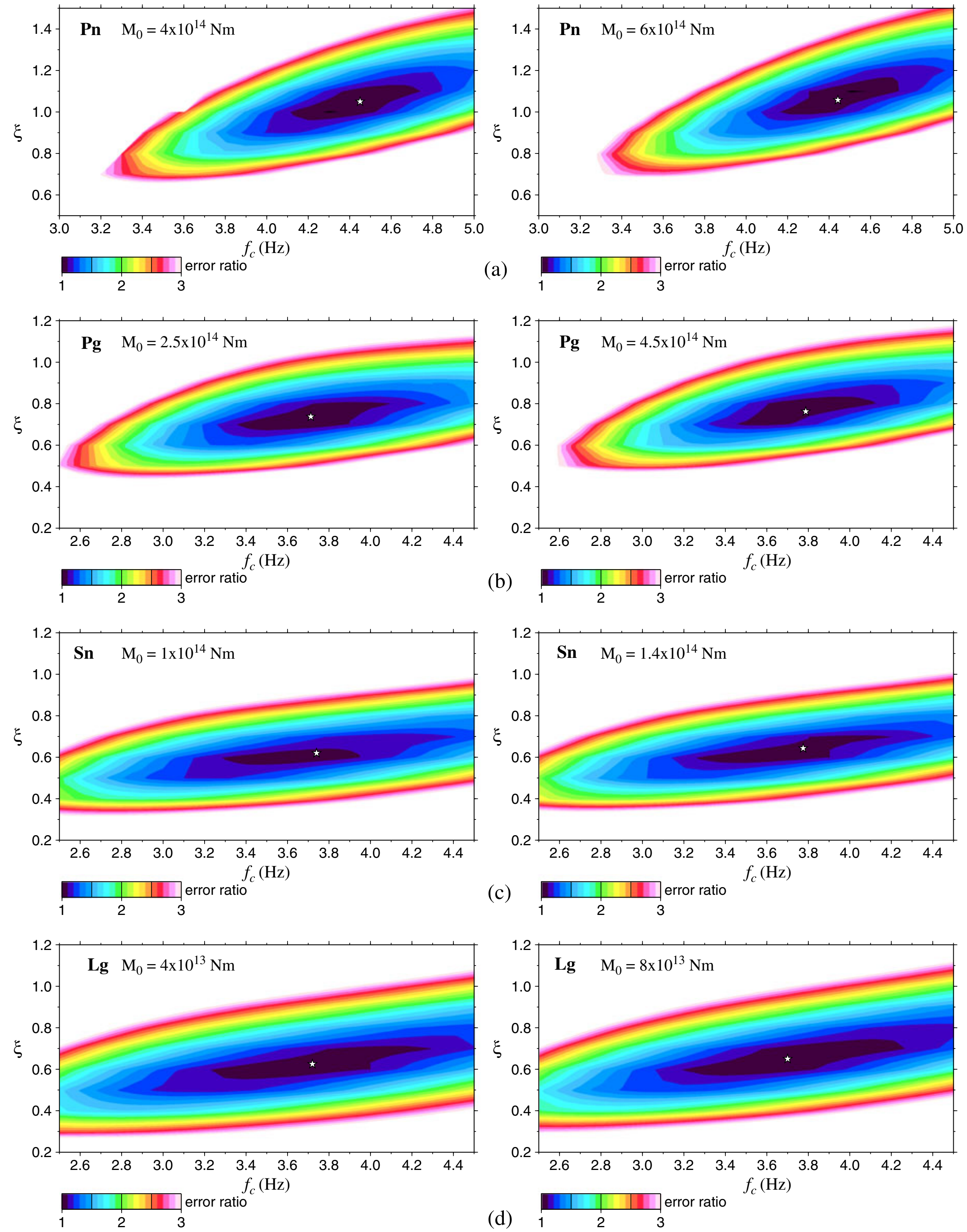

Fig. 5 Estimation of misfit errors as function of corner frequency (f_c) and overshoot parameter (ξ) for various given apparent moments: **a** *Pn*, **b** *Pg*, **c** *Sn*, and **d** *Lg*. The model parameters (f_c, ξ) are determined to be consistent for changes of implemented moments at all phases

parameters are chosen as the representative path parameters.

5 Process and analysis

The velocities v_g in Eq. 1 are set to be 7,950 m/s for *Pn*, 6,050 m/s for *Pg*, 4,550 m/s for *Sn*, and 3,500 m/s for *Lg* (Hong and Kang 2009; Hong and Rhie 2009). The *P* and *S* wave velocities in the source and receiver regions, v_s and v_r, are set to be 5,670 and 3,273 m/s, respectively. The density in the source region (ρ_s) is assumed to be 2,580 kg/m^3.

The *Pn* phase is collected from wave trains in a travel-time range between $d/7.95 + 5$ and $d/6.6 + 0.8$ s, where d is the epicentral distance in kilometer. The waveforms in a travel-time range between $d/6.05 + 0.8$ and $d/5.0 + 11.0$ s are analyzed for *Pg*, those between $d/4.50 + 11.0$ and $d/3.7 + 0.5$ s are for *Sn*, and those between $d/3.57 + 0.5$ and $d/3.15$ s are for *Lg* (Hong and Rhie 2009). A 4.5-s long moving time window with 0.2-s-long cosine tapers at both ends is used to collect waveforms of regional phases.

The representative spectrum of a regional phase is calculated by stacking the spectra of waveforms in moving time windows. The spectra are stacked in the frequency range of 1–8 Hz considering the frequency contents of regional seismic waves and the size of time window. Here, the levels of stacked spectral amplitudes vary with the moving-time-window size and the prescribed travel-time ranges. Note that the lengths of wave trains analyzed are determined by the prescribed travel-time ranges. Thus, the lengths of wave trains analyzed increase with distance. It is noteworthy that only the apparent moments can be determined based on the stacked spectral amplitude that changes with the moving-time-window size and the prescribed travel-time range. The frequency interval in the stacked spectra is 0.01 Hz. The source spectra are inverted based on the stacked spectra between 1 and 8 Hz. The number of discrete frequencies (m in Eq. 6) is 701.

We determine the model parameters using the two-step inversion approach. In the first step of inversion, we determine apparent moments yielding Q parameters that are consistent with previous studies (Kim et al. 1999; Chung and Sato 2001; Hong and Rhie 2009; Hong 2010a). We then determine the corner frequency (f_c) and overshoot parameter (ξ) with implementation of the apparent moments determined in the first step of inversion. The source-spectral parameters are grid-searched in every 0.1 Hz for f_c and every 0.1 for ξ. The best-fit set of f_c and ξ is determined by averaging the discrete parameters satisfying a given level of misfit error that is set to be the 1.1 times the minimum misfit error. This procedure allows us to stably determine the model parameters in the inversion based on grid-searching scheme.

In the inversion of model parameters, there are trade-offs between the apparent moment and quality factors. Thus, when attenuation is overestimated, the apparent moment is determined to be larger than the true value. Similarly, the apparent moment is determined to be lower than the true value when the attenuation is underestimated. On the other hand, the corner frequency (f_c) and overshoot parameter (ξ) are estimated to be nearly constant for change of moment (Fig. 5, Table 2). The consistent determination of f_c and ξ for different M_0 verifies the two-step approach.

Table 2 Variation of source-spectral parameters of regional phases for changes of apparent moments (M_0)

Phase	M_0 (N·m)	f_c (Hz)	ξ
Pn	4.0×10^{14}	4.45	1.05
	5.0×10^{14}	4.44	1.05
	6.0×10^{14}	4.44	1.06
Pg	2.5×10^{14}	3.71	0.74
	3.5×10^{14}	3.75	0.75
	4.5×10^{14}	3.79	0.76
Sn	1.0×10^{14}	3.74	0.62
	1.2×10^{14}	3.76	0.64
	1.4×10^{14}	3.78	0.64
Lg	4.0×10^{13}	3.72	0.63
	6.0×10^{13}	3.71	0.65
	8.0×10^{13}	3.70	0.65

The corner frequencies (f_c) and overshoot parameters (ξ) are determined to be nearly constant for changes of M_0

In this study, the source-spectral inversions are based on a large number of waveforms (801 waveforms) from stations on various paths, in order to stably determine the source parameters. We find that the source parameters rarely vary with inclusion or exclusion of particular data when large numbers of data are analyzed in the inversion. This is because the source spectra are determined based on the full data set, and inclusion or exclusion of particular records hardly causes significant variation in the inverted source parameters.

Similarly, the inverted source-spectral parameters are hardly influenced by inclusion of waveform records with low signal-to-noise ratios in the analysis. This is because such waveforms with low signal-to-noise ratios are determined to have low Q values along the paths in the inversion. It is also noteworthy that the path parameters ($Q_{0,j}$, η_j) are determined by path, and they are determined to be constant for given M_0, f_c, and ξ regardless of addition or removal of data from other stations. This is because the path parameters for a certain path are determined based only on the corresponding waveform. Thus, the path parameters for a certain path are determined independently from those for other paths.

6 Regional source spectra

The corner frequencies (f_c) are determined to be 4.44 Hz for *Pn*, 3.75 Hz for *Pg*, 3.76 Hz for *Sn*, and 3.71 Hz for *Lg* (Table 3). The *Pn* phase displays a slightly higher corner frequency than the other phases that present comparable corner frequencies. This *Pn* corner frequency is smaller than that of the 2006 UNE (Hong and Rhie 2009). The observation agrees with the general relationship between the corner frequency and event size (e.g., Atkinson 1993; Xie and Patton 1999).

The overshoot parameter (ξ) is estimated to be 1.05 for *Pn*, 0.75 for *Pg*, 0.64 for *Sn*, and 0.65 for *Lg*. The *Pn* phase displays the largest overshoot parameter. Such a large overshoot feature is consistent with the 2006 UNE (Hong and Rhie 2009), suggesting that the source may be associated with a strong explosive source such as an underground nuclear explosion. We, however, observe relatively weak overshoot features in the other phases (*Pg*, *Sn*, and *Lg*). The observation suggests that the *Pn* phase may be more suitable for investigation of UNE source properties than other phases.

The inverted source spectra from single records are observed to be similar, and their standard deviations are found to be small (Fig. 6). The average source spectra match well with the theoretical models that are calculated based on the inverted source-spectral parameters, particularly at frequencies of 1.5 Hz or higher. The fractional differences between the observed and theoretical source spectra based on the UNE model present the maximum fractional differences of 2.0–2.6 % and the average fractional differences of 0.9–1.0 % at frequencies of 1.5–7.5 Hz for all regional phases. The high similarity among the source spectra estimated at individual stations supports the stability of the inversion. This observation also suggests that records with low signal-to-noise ratios can be applied without degrading the stability of source-spectral inversion.

Table 3 Inverted source-spectral parameters of regional phases from the 2009 North Korean UNE

Phase	M_0 (N·m)	f_c (Hz)	ξ
Pn	5.0×10^{14}	4.44	1.05
Pg	3.5×10^{14}	3.75	0.75
Sn	1.2×10^{14}	3.76	0.64
Lg	6.0×10^{13}	3.71	0.65

The apparent moments (M_0), corner frequencies (f_c), and overshoot parameters (ξ) are presented

7 Seismic discrimination based on source-spectral fitness

The UNE source is discriminated by comparing the estimated source spectra with theoretical models. We find that the source spectra inverted based on a UNE source-spectral model matches well with the theoretical model (Fig. 6). We additionally perform a source-spectral inversion

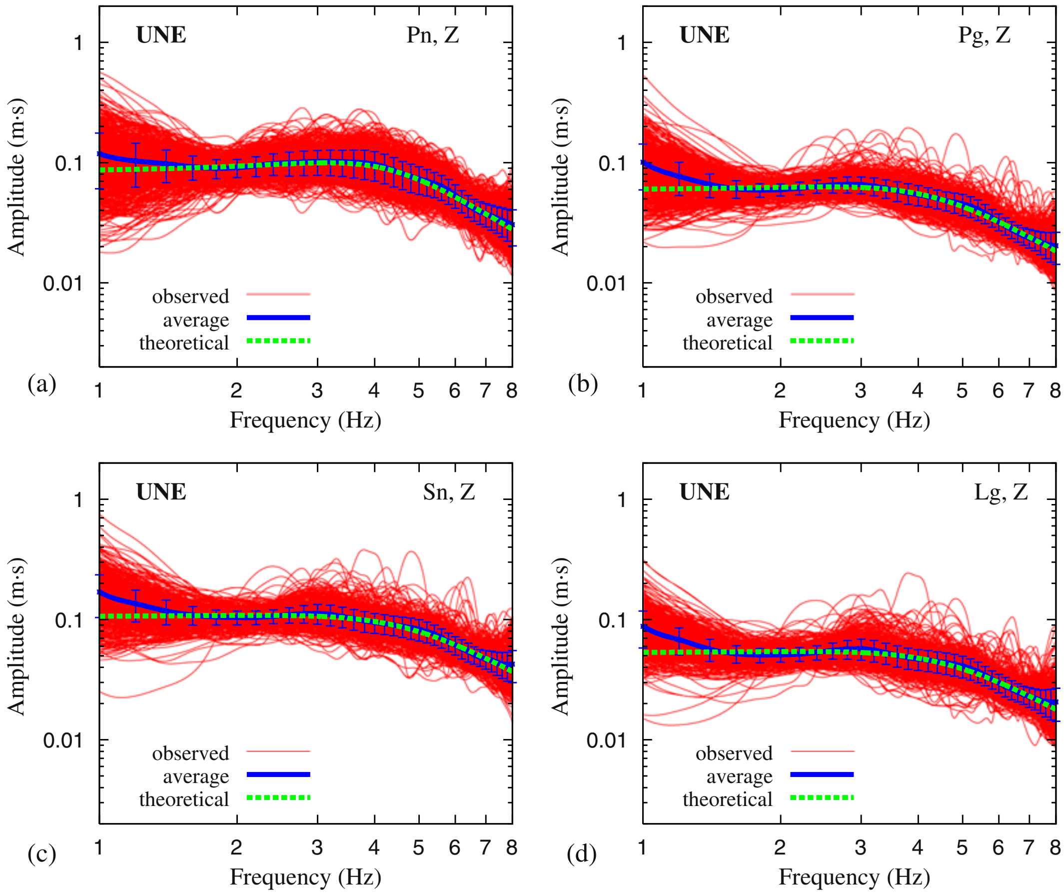

Fig. 6 Source spectra of regional phases from the 2009 UNE: **a** *Pn*, **b** *Pg*, **c** *Sn* and **d** *Lg*. The source spectra inverted from single records are presented by *red lines*, and their mean variations along with standard deviations are marked with *blue lines*. The theoretical source spectra are presented by *green lines*. The inverted source spectra match well with the theoretical source spectra for all regional phases

based on an earthquake source-spectral model to evaluate the model-dependent source-spectral fitness.

We apply the Brune's earthquake source-spectral model that is given by (Brune 1970; Stevens and Day 1985)

$$S(f) = \frac{M_0 R_{\theta\phi}}{4\pi\sqrt{\rho_s \rho_r v_s^5 v_r}\left(1 + f^2/f_c^2\right)}, \quad (8)$$

where $R_{\theta\phi}$ is an amplitude scaling factor for source radiation pattern, and ρ_r and v_r are the density and seismic velocity in the receiver region, respectively. The radiation pattern $R_{\theta\phi}$ is set to be 0.63 for P phases (Pn, Pg) and 0.43 for S phases (Sn, Lg) (Hong and Rhie 2009).

We first compare the Q factors with those from inversion based on the UNE source-spectral model and examine the model dependence on the inverted Q factors. We measure the fractional Q^{-1} differences between the two results (Fig. 7). The fractional differences are calculated by

$$\gamma = \frac{Q_{\mathrm{EQ}}^{-1} - Q_{\mathrm{UNE}}^{-1}}{Q_{\mathrm{UNE}}^{-1}}, \quad (9)$$

where Q_{EQ} is the Q parameter from analysis based on an earthquake source-spectral model, and Q_{UNE} is the Q parameter from analysis based on the UNE source-spectral model. We find that the fractional Q^{-1} differences are close to zero for all phases, suggesting high similarity of the

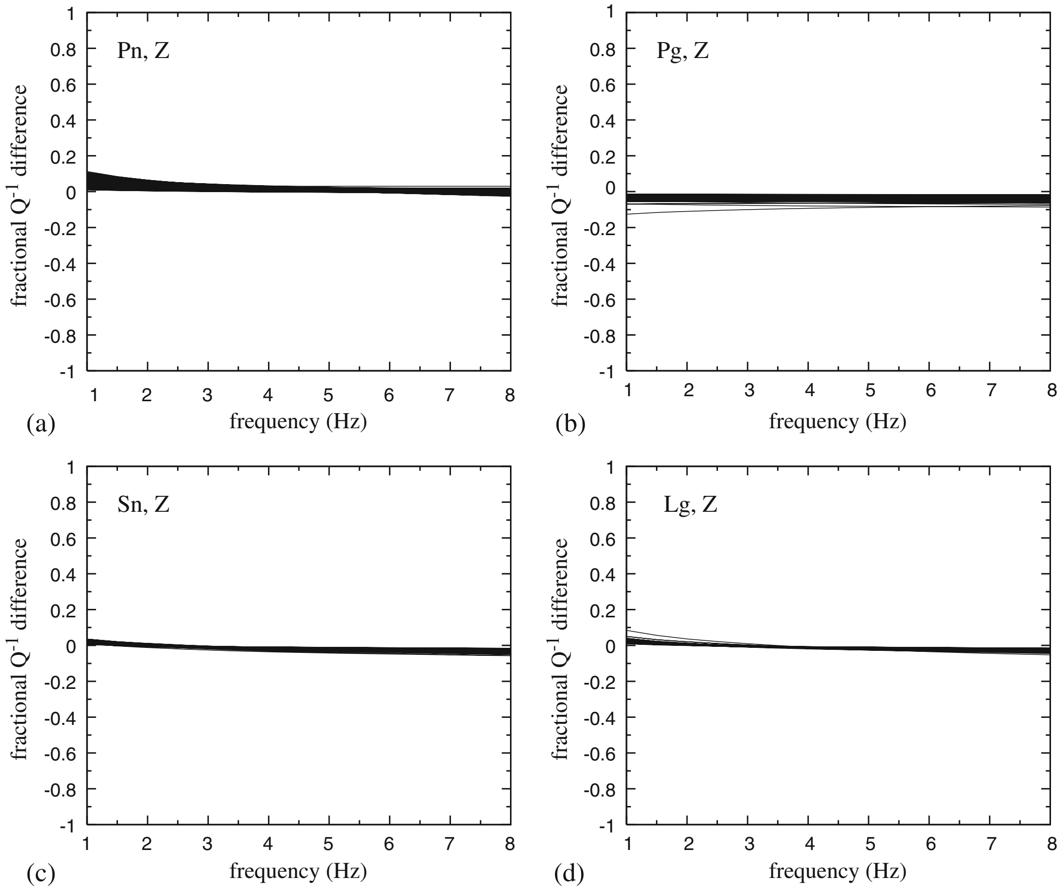

Fig. 7 Fractional Q^{-1} differences between the inversions based on a UNE source-spectral model and those based on an earthquake source-spectral model: **a** *Pn*, **b** *Pg*, **c** *Sn*, and **d** *Lg*. The fractional Q^{-1} differences are observed to be close to zero for all frequencies, suggesting that the path properties are determined to be consistent for changes of source-spectral models

Q values between the results. The observation suggests that path parameters (Q) are determined to be consistent regardless of the source-spectral model implemented, suggesting stable separation of path properties from waveform records. The observation also supports the stability of the inversion scheme.

We find changes in apparent moments and corner frequencies due to implementation of a different source-spectral model. The apparent moments (M_0) are determined to be 1.3×10^{15} Nm for *Pn*, 6.6×10^{14} Nm for *Pg*, 3.5×10^{14} Nm for *Sn*, and 1.8×10^{14} Nm for *Lg*. The corner frequencies are determined to be similar between the phases, which are 4.8 Hz for *Pn*, 4.9 Hz for *Pg*, 5.0 Hz for *Sn*, and 4.8 Hz for *Lg*.

The inverted source spectra display the characteristic overshoot feature in all phases, particularly strong in *Pn* (Fig. 8). The stacked source spectra of regional phases are compared with the theoretical Brune source spectra. The inverted source spectra are found to match poorly with the theoretical Brune source spectra, particularly around the corner frequencies where characteristic spectral overshooting is observed (Fig. 8).

The fractional differences between the observed and theoretical source spectra based on the Brune source-spectral model present maximum fractional differences of 9.7 % and average fractional differences of 5.3 % for *Pn* at frequencies of 1.5–7.5 Hz. Also, the maximum fractional differences are determined to be 4.7–5.2 %, and

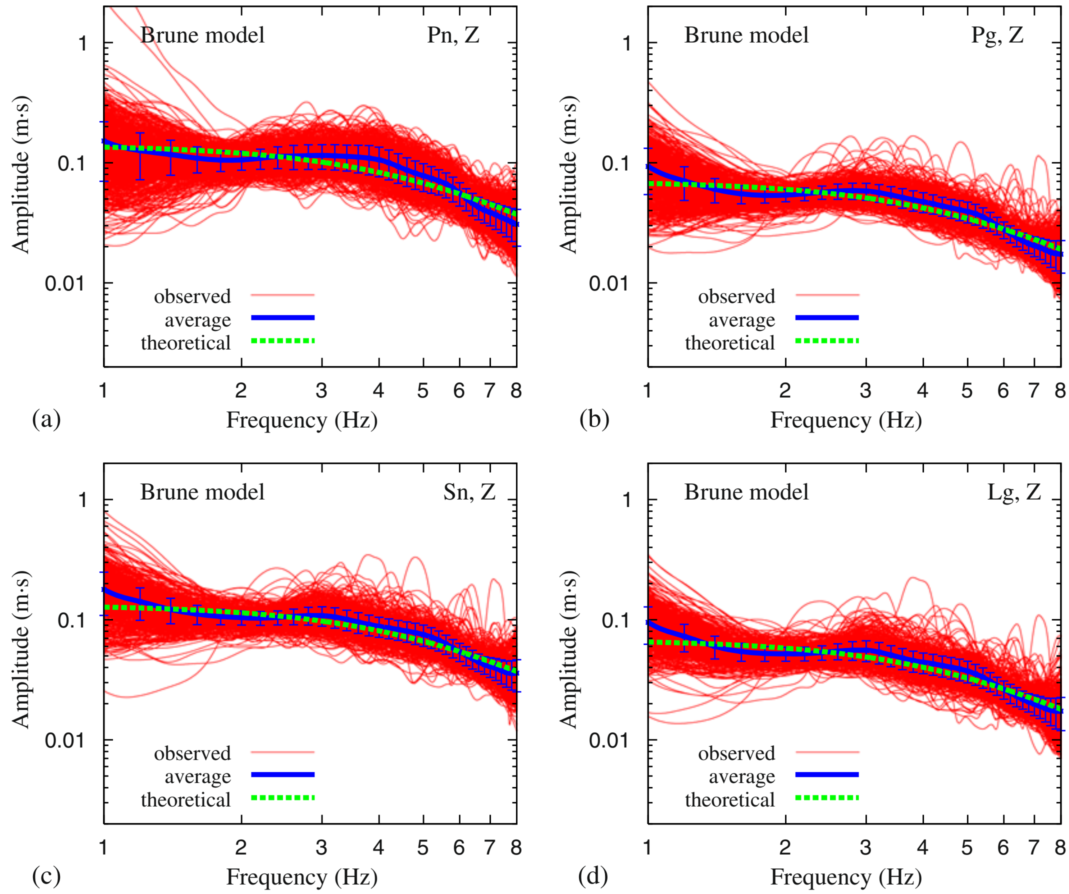

Fig. 8 Source spectra of regional phases that are inverted with an earthquake source-spectral model: **a** *Pn*, **b** *Pg*, **c** *Sn*, and **d** *Lg*. The source spectra inverted from single records are presented by *red lines*, and their mean variations along with standard deviations are marked with *blue lines*.The theoretical source spectra are presented by *green lines*. The inverted source spectra of *P* phases (*Pn*, *Pg*) match poorly with the theoretical source spectra

the average fractional differences are estimated to be 2.8–3.2 % for the other phases. These fractional differences are higher than those from inversions based on the UNE source-spectral model. The observation suggests that comparisons between observed and theoretical source spectra may allow us to discriminate between UNEs and earthquakes.

8 Seismic discrimination based on *P/S* source-spectral ratios

In principle, *S* energy is rarely radiated from explosion sources. However, it is known that the *S* waves are developed by various secondary sources such as rock cracking (Massé 1981), tectonic release (Toksöz and Kehrer 1972; Ekström and Richards 1994), spalling (Stump 1985; Day and McLaughlin 1991), S* (Gutowski et al. 1984; Vogfjörd 1997), *P*-to-*S* scattering (Rodgers et al. 2010), and *Rg*-to-*S* scattering (Gupta et al. 1992; Myers et al. 1999). Also, the amplitudes of seismic waves are highly influenced by medium properties along raypaths (Fig. 4). Thus, it is often found that simple *P/S* amplitude ratios of single time records may not be useful for discrimination of source types.

Source spectra of phases present the phase strengths in the source, in which the path effects are not included. Here, we use the *P/S* source-spectral ratios instead of simple *P/S* amplitude ratios. The *P/S* source-spectral ratios are calculated using the inverted source spectra based on the UNE source model. We calculate four pairs of *P/S* source-spectral ratios: *Pn/Sn*, *Pn/Lg*, *Pg/Sn*, and *Pg/Lg* source-spectral ratios (Fig. 9). The *P/S* source-spectral ratios are determined to be nearly constant at frequencies of 1–8 Hz. The *P/S* source-spectral ratios are compared with the theoretical source-spectral ratios. We find that the stacked *P/S* source-spectral ratios match well with the theoretical source-spectral ratios.

We additionally calculate the *P/S* source-spectral ratios using the source spectra inverted with an earthquake source-spectral model (Brune's model). It is intriguing to note that the *P/S* source-spectral ratios based on the Brune's model are observed to be close to those based on the UNE model (Fig. 10). This feature may be associated with the fact that the path parameters (Q) are inverted uniquely regardless of the type of source model applied. Thus, the source spectra are inverted to be consistent for different source models.

The *P/S* source-spectral ratios of the 2009 UNE are compared with those of a nearby m_b4.1 earthquake. The earthquake occurred in a location about 82 km southwest from the UNE (Fig. 1, Table 1). The source-spectral parameters of the earthquake are collected from Hong and Rhie (2009). We find large differences in *P/S* source-spectral ratios between the 2009 UNE and the

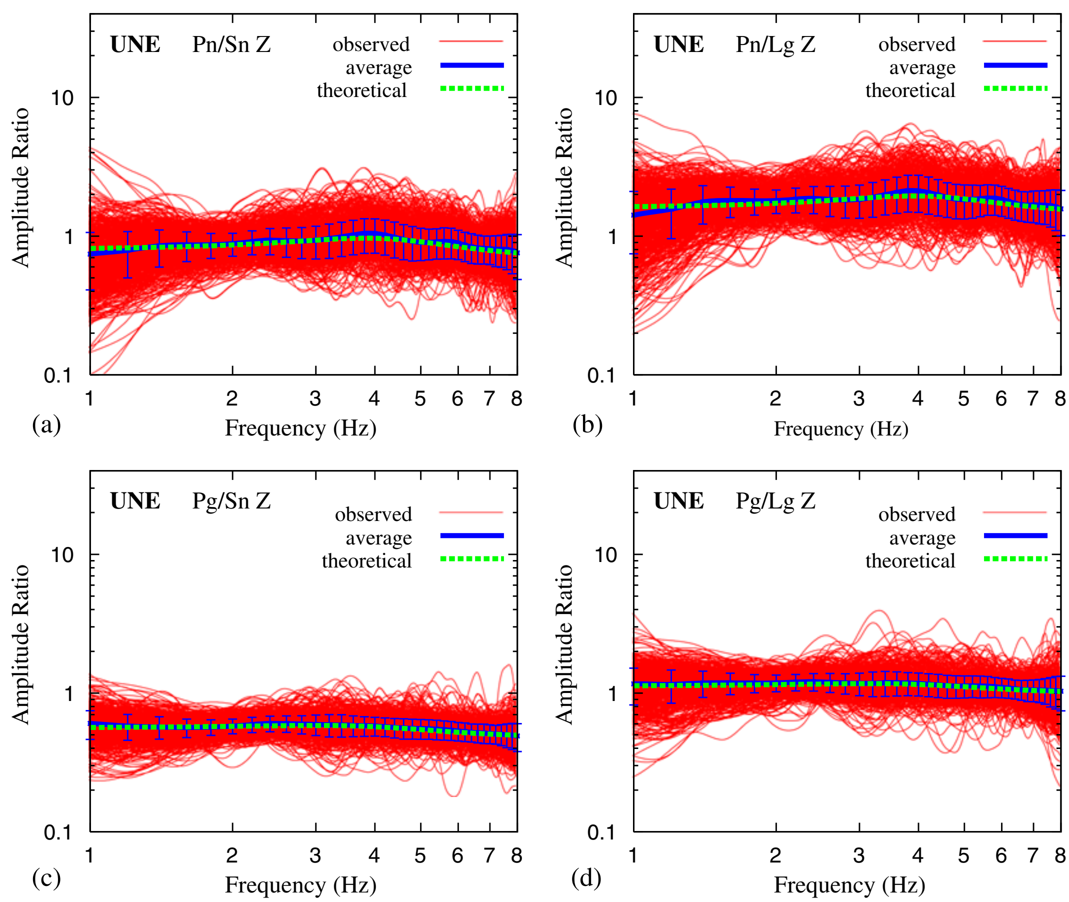

Fig. 9 *P/S* source-spectral amplitude ratios for the 2009 UNE: **a** *Pn/Sn*, **b** *Pn/Lg*, **c** *Pg/Sn*, and **d** *Pg/Lg*. The *P/S* source-spectral amplitude ratios for every station are presented by *red lines*. The mean *P/S* ratios and the standard deviations are presented by *blue lines*. The theoretical *P/S* source-spectral amplitude ratios are displayed by *green lines*. The mean *P/S* ratios match well with the theoretical *P/S* ratios. The mean *P/S* ratios are determined to be nearly constant at frequencies of 1–8 Hz

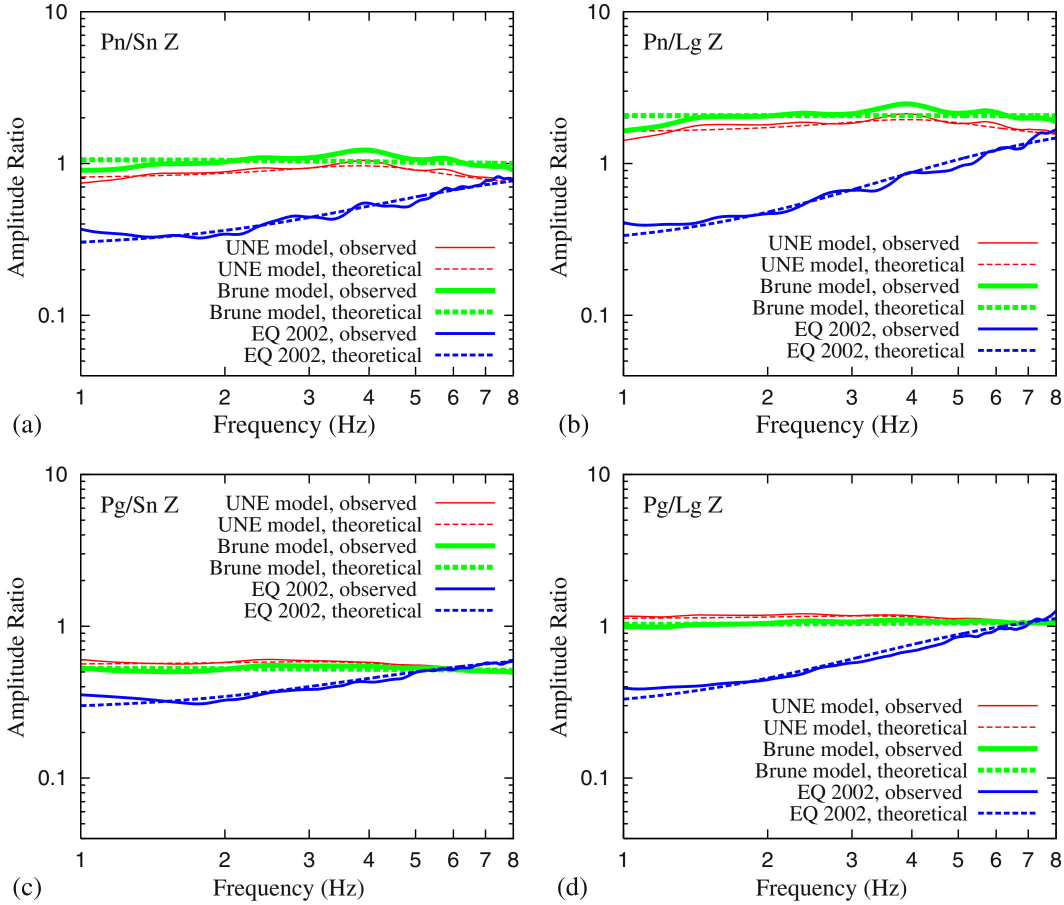

Fig. 10 Comparisons between *P/S* source-spectral amplitude ratios from analyses based on the UNE source model and those from analyses based on an earthquake source model: **a** *Pn/Sn*, **b** *Pn/Lg*, **c** *Pg/Sn*, and **d** *Pg/Lg*. The *P/S* ratios are determined to be consistent for changes of implemented source-spectral models

earthquake in the frequency range of 1–5 Hz. This observation suggests that *P/S* source-spectral ratios are effective for discrimination of UNE.

9 Discussion and conclusions

Discrimination of UNE is a crucial task in nuclear-monitoring seismology. Seismic discrimination is often based on the comparison of waveform properties between an unidentified source and known natural earthquakes of comparable magnitudes. Thus, when such comparable earthquakes are not available, it is difficult to discriminate the UNEs. This is particularly challenging for small or moderate-sized UNEs that are typically observed up to regional distances. This is because the regional waveforms are highly influenced by crustal structures.

The regional waveforms for the North Korean UNEs are observed to be highly path-dependent due to complex crustal structures around the Korean Peninsula that is located in the northeastern Eurasian plate margin. The relative amplitudes of major phases at common stations are observed to be highly varying between the UNEs, suggesting difficulty of direct analysis of single records for discrimination of source type in regions with complex crustal structures. Thus, it is highly desired in source discrimination to analyze the source properties with correction of path effects.

In this study, the source-spectral parameters and path parameters are inverted from dense records. A two-step inversion approach was found to be stable and effective for the inversion. It is observed that the corner frequencies of regional source spectra appear to be comparable among different phases. The *P* overshoot parameters are determined to be slightly larger than the *S* overshoot parameters, which is consistent with previous studies (e.g., Xie and Patton 1999). The path parameter (Q) is determined to be consistent for change of source-spectral models, suggesting stable determination of the Q parameter. This feature supports the validity of the two-step inversion approach.

The inverted source spectra based on a UNE model match well with the theoretical source spectra. The average fractional differences between the observed and theoretical source spectra are found to be 0.9–1.0 % at frequencies of 1.5–7.5 Hz for all phases. On the other hand, the inverted source spectra based on an earthquake model are found to match poorly with the theoretical source spectra. The average fractional differences between the observed and theoretical source spectra are found to be 5.3 % for *Pn* and 2.8–3.2 % for the other phases. The misfit errors of the observed source spectra with respect to the theoretical source spectra based on an earthquake model are three to six times larger than those with respect to the theoretical source spectra based on a UNE model. The observation suggests that the fitness degree between the inverted and theoretical source spectra can be used as an effective UNE discriminant. The source discrimination based on the source-spectral fitness may be particularly useful for regions with rare natural earthquakes with magnitudes comparable to those of UNEs.

We also compare the *P/S* source-spectral ratios of the 2009 UNE with those of a nearby natural earthquake. We find large differences in the *P/S* source-spectral ratios between the UNE and the nearby earthquake in the frequency range of 1–5 Hz. This observation suggests that the *P/S* source-spectral ratios are applicable for regions with complex crustal structures. It is also found that the *P/S* source-spectral ratios are similar between the results based on a UNE source-spectral model and those based on an earthquake source-spectral model. The observation suggests that the source-spectral ratios can be estimated uniquely regardless of the source-spectral model implemented.

Acknowledgements I am grateful to the Korea Meteorological Administration, the Korea Institute of Nuclear Safety, the National Research Institute for Earth Science and Disaster Prevention in Japan, and the Incorporated Research Institutions for Seismology, for making seismic data available. I thank two anonymous reviewers and the associate editor, Dr. Thomas Braun, for valuable review comments and suggestions that improved the presentation of paper. This work was supported by the Korea Meteorological Administration Research and Development Program under Grant CATER 2012-8050.

References

Aki K, Bouchon M, Reasenberg P (1974) Seismic source function for an underground nuclear explosion. Bull Seismol Soc Am 64:131–148

Atkinson GM (1993) Earthquake source spectra in Eastern North America. Bull Seismol Soc Am 83:1778–1798

Bonner J, Herrmann RB, Harkrider D, Pasyanos M (2008) The surface wave magnitude for the 9 October 2006 North Korean nuclear explosion. Bull Seismol Soc Am 98(5):2498–2506

Brune JN (1970) Tectonic stress and the spectra of seismic shear waves from earthquakes. J Geophys Res 75(26):4997–5009

Brune JN, Pomerory PW (1963) Surface wave radiation patterns for underground nuclear explosions and small magnitude earthquakes. J Geophys Res 68:5005–5028

Burdick LJ, Wallace T, Lay T (1984) Modeling near-field and teleseismic observations from the Amchitka test site. J Geophys Res 89(B6):4373–4388

Chough SK, Kwon S-T, Ree J-H, Choi DK (2000) Tectonic and sedimentary evolution of the Korean peninsula: a review and new view. Earth-Sci Rev 52:175–235

Chun K-Y, Henderson GA (2009) Lg attenuation near the North Korean border with China, Part II: model development from the 2006 nuclear explosion in North Korea. Bull Seismol Soc Am 99(5):3030–3038

Chung TW, Sato H (2001) Attenuation of high-frequency P and S waves in the crust of Southeastern South Korea. Bull Seismol Soc Am 91(6):1867–1874

Day SM, McLaughlin KL (1991) Seismic source representations for spall. Bull Seismol Soc Am 81(1):191–201

Denny MD, Johnson LR (1991) The explosion seismic source function: models and scaling laws reviewed. In: Taylor SR, Patton HJ, Richards PG (eds) Explosion source phenomenology, geophysical monograph, vol 65. American Geophysical Union, pp 1–24

Ekström G, Richards PG (1994) Empirical measurements of tectonic moment release in nuclear explosions from teleseismic surface waves and body waves. Geophys J Int 117:120–140

Fisk MD (2007) Corner frequency scaling of regional seismic phases for underground nuclear explosions at the Nevada test site. Bull Seismol Soc Am 97(3):977–988

Ford SR, Dreger DS, Walter WR (2009) Source analysis of the Memorial Day explosion, Kimchaek, North Korea. Geophys Res Lett 36:L21304. doi:10.1029/2009GL040003

Gupta IN, Chan WW, Wagner RA (1992) A comparison of regional phases from underground nuclear explosions at East Kazakh and Nevada test sites. Bull Seismol Soc Am 82:352–382

Gutowski PR, Hron F, Wagner DE, Treitel S (1984) S*. Bull Seismol Soc Am 74(1):61–78

He X, Hong T-K (2010) Evidence for strong ground motion by waves refracted from the Conrad discontinuity. Bull Seismol Soc Am 100(3):1370–1374

Hong T-K (2010a) Lg attenuation in a region with both continental and oceanic environments. Bull Seismol Soc Am 100(2):851–858

Hong T-K (2010b) Regional and teleseismic analysis of underground nuclear explosion waveforms and constraints for shear-wave excitation mechanisms. J Geophys Res 115:B06306. doi:10.1029/2009JB006368

Hong T-K (2011) Seismic investigation of the 26 March 2010 sinking of the South Korean naval vessel Cheonanham. Bull Seismol Soc Am 101(4):1554–1562

Hong T-K (2012) Lg body-wave magnitude scaling for the continental margin around Korea and Japan. Pure Appl Geophys 169(4):641–658

Hong T-K, Baag C-E, Choi, H, Sheen D-H (2008) Regional seismic observations of the October 9, 2006 underground nuclear explosion in North Korea and the influence of crustal structure on regional phases. J Geophys Res 113:B03305. doi:10.1029/2007JB004950

Hong T-K, Kang T-S (2009) Pn traveltime tomography of the paleo-continental-collision and rifting zone around Korea and Japan. Bull Seismol Soc Am 99(1):416–421

Hong T-K, Lee K (2012) mb(Pn) scale for the Korean Peninsula and site-dependent Pn amplification. Pure Appl Geophys 169(11):1963–1975

Hong T-K, Rhie J (2009) Regional source scaling of the 9 October 2006 underground nuclear explosion in North Korea. Bull Seismol Soc Am 99(4):2523–2540

Hong T-K, Xie J (2005) Phase composition of regional seismic waves from underground nuclear explosions. J Geophys Res 110:B12302. doi:10.1029/2005JB003753

Kennett BLN, Furumura T (2001) Regional phases in continental and oceanic environments. Geophys J Int 146(2):562–568

Kim SK, Jun MS, Kim JK (1999) Attenuation of P waves in the Kyungsang Basin, Southeastern Korea. J Geol Soc Kor 35:223–228 (in Korean)

Kim W-Y, Richards PG (2007) North Korean nuclear test: seismic discrimination at low yield. Eos Trans AGU 88(14). doi:10.1029/ 2007EO140002

Koper KD, Herrmann RB, Benz HM (2008) Overview of open seismic data from the North Korean event of 9 October 2006. Seismol Res Lett 79(2):178–185

Lay T, Helmberger DV, Harkrider DG (1984) Source models and yield-scaling relations for underground nuclear explosions at Amchitka island. Bull Seismol Soc Am 74:843–862

Massé RP (1981) Review of seismic source models for underground nuclear explosions. Bull Seismol Soc Am 71:1249–1268

Mueller RA, Murphy JR (1971) Seismic characteristics of underground nuclear detonations. Bull Seismol Soc Am 61(6):1675–1692

Myers SC, Walter WR, Mayeda K, Glenn L (1999) Observations in support of Rg scattering as a source for explosion S waves: regional and local recordings of the 1997 Kazakhstan depth of burial experiment. Bull Seismol Soc Am 89:544–549

Paige CC, Saunders MA (1982) LSQR: an algorithm for sparse linear equations and sparse least squares. ACM Trans Math Softw 8:43–71

Patton HJ (2001) Regional magnitude scaling, transportability, and Ms:mb discrimination at small magnitudes. Pure Appl Geophys 158:1951–2015

Patton HJ, Taylor SR (2008) Effects of shock-induced tensile failure on m_b-M_s discrimination: contrasts between historic nuclear explosions and the North Korean test of 9 October 2006. Geophys Res Lett 35:L14301. doi:10.1029/2008GL034211

Richards PG, Kim W-Y (2007) Seismic signature. Nat Phys 3:4–6

Rodgers AJ, Petersson NA, Sjogreen B (2010) Simulation of topographic effects on seismic waves from shallow explosions near the North Korean nuclear test site with emphasis on shear wave generation. J Geophys Res 115:B11309. doi:10.1029/2010JB007707

Sereno Jr TJ, Bratt SR, Bache TC (1988) Simultaneous inversion of regional wave spectra for attenuation and seismic moment in Scandinavia. J Geophys Res 93(B3):2019–2035

Shin JS, Sheen D-H, Kim G (2010) Regional observations of the second North Korea nuclear test on 2009 May 25. Geophys J Int 180:243–250

Stevens JL, Day SM (1985) The physical basis of m_b : M_s and variable frequency magnitude methods for earthquake/explosion discrimination. J Geophys Res 90(B4):3009–3020

Stump BW (1985) Constraints on explosive sources with spall from near-source waveforms. Bull Seismol Soc Am 75:361–377

Taylor SR, Denny MD, Vergino ES Glaser RE (1989) Regional discrimination between NTS explosions and western U.S. earthquakes. Bull Seismol Soc Am 79:1142–1176

Toksöz MN, Kehrer HH (1972) Tectonic strain release by underground nuclear explosions and its effect on seismic discrimination. Geophys j R Astron Soc 31:141–161

Vogfjörd KS (1997) Effects of explosion depth and earth structure on the excitation of Lg waves: S* revisited. Bull Seismol Soc Am 87(5):1100–1114

Walter WR, Matzel E, Pasyanos ME, Harris DB, Gok R, Ford SR (2007) Empirical observations of earthquake-explosion discrimination using P/S ratios and implications for the sources of explosion S-waves. In: 29th monitoring research review: ground-based nuclear explosion monitoring technologies. The National Nuclear Security Administration, LA-UR-07-5613, pp 684–693

Walter WR, Taylor SR (2002) A revised magnitude and distance amplitude correction (MDAC2) procedure for regional seismic discriminants: theory and testing at NTS, UCRL-ID-146882, LA-UR-02-1008. Lawrence Livermore National Laboratory, pp 13

Weichert DH (1971) Short-period spectral discriminant for earthquake-explosion differentiation. Z Geophys 37:147–152

Xie J, Patton HJ (1999) Regional phase excitation and propagation in the Lop or region of central Asia and implications for P/Lg discriminants. J Geophys Res 104(B1):941–954

Zhao L-F, Xie X-B, Wang W-M, Yao Z-X (2008) Regional seismic characteristics of the 9 October 2006 North Korean nuclear test. Bull Seismol Soc Am 98(6):2571–2589

Zhu T, Chun K-Y, West GF (1991) Geometrical spreading and Q of Pn waves: an investigative study in Eastern Canada. Bull Seismol Soc Am 81(3):882–896